PERGAMON

Journal of Structural Geology 25 (2003) 263–275

JOURNAL OF STRUCTURAL GEOLOGY

www.elsevier.com/locate/jsg

Development of antitaxial strain fringes during non-coaxial deformation: an experimental study

Daniel Koehn[a,b,*], Paul D. Bons[b], Cees W. Passchier[b]

[a]*Department of Geology, University of Oslo, Blindern, N-0271 Oslo, Norway*
[b]*Institut für Geowissenschaften, Johannes Gutenberg Universität, 55099 Mainz, Germany*

Received 23 January 2001; received in revised form 25 January 2002; accepted 5 February 2002

Abstract

Strain fringes were modelled experimentally around wooden objects in a simple-shear box containing Polydimethylsiloxane (PDMS). The fringes were made of paraffin wax that was periodically poured into dilated sites next to the core-object and left to crystallise. In the experiments fringes and core-object rotated at similar decreasing rotation rates relative to extensional incremental stretching axes (ISA) of flow and rotated relative to each other by small amounts. Fringes did not necessarily open parallel to ISA due to interactions between fringes and core-object. Therefore, neither displacement-controlled fibres nor object-centre paths can be expected to record the exact orientation of the extensional ISA, but only give estimates. Existing methods to calculate finite strain were applied to the experimental fringes. These methods generally underestimate the actual finite shear-strain. This study illustrates that different final fringe shapes can develop in the same shear zone depending on core-object shape and its initial orientation with respect to the shear zone boundary. A classification of final fringe shapes is presented based on the initial orientation of elongate core-objects.

Keywords: Strain fringes; Strain analysis; Fibres; Rotation; Translation

1. Introduction

A rigid object such as a pyrite crystal in a deforming matrix causes perturbations in the flow pattern, which can lead to growth of crystalline aggregates close to the object (Mügge, 1928; Pabst, 1931) in the direction of the extensional instantaneous stretching axes (ISA). Such newly formed crystalline aggregates are known as *pressure-* and *strain shadows* or *strain fringes* (Pabst, 1931; Ramsay and Huber, 1983; Passchier and Trouw, 1996). A strain fringe is defined as a crystalline aggregate close to an object with a distinct direction of crystal growth and sharp boundaries to the matrix (Fig. 1) whereas a strain shadow contains blocky crystals and has fuzzy boundaries, while the direction of crystal growth is not clear. The central object between two strain fringes is termed a *core-object* and the whole structure (core-object and fringes) a *fringe structure* (Koehn et al., 2000). Strain fringes are of special importance since fibres (crystals with a high length to width ratio) in these fringes are thought to grow syn-kinematic and to record part of the progressive deformation history of the host-rock. Therefore they have been used by many geologists for structural analysis from determination of shear sense to advanced kinematic fibre analysis (e.g. Zwart and Oele, 1966; Elliott, 1972; Durney and Ramsay, 1973; Wickham, 1973; Beutner et al., 1988; Fisher 1990; Spencer, 1991; Aerden, 1996 and others mentioned in Koehn et al., 2000).

Strain fringes have been classified into *syntaxial* or *antitaxial* and *deforming* or *non-deforming* fringes (Ramsay and Huber, 1983; Passchier and Trouw, 1996). Antitaxial non-deforming strain fringes are the subject of this study since they are the most common type in nature. They contain fibres that grow towards the core-object so that growth takes place at the fringe/core-object boundary and fringes remain rigid. Fibres within these fringes are assumed to grow displacement-controlled (Ramsay and Huber, 1983) and to follow relative core-object/fringe movements (*translation and rotation* in the terminology of Means (1976, 1994)).

Even though the development of antitaxial strain fringes has been the subject of recent studies, it is still not clear (1) how fringes and core-object rotate and translate relative to an external reference frame and (2) how reliable a kinematic fibre analysis of these structures is (Spencer, 1991). In order to link fibre growth direction in strain fringes to fringe opening direction and rotation a fibre growth model is needed,

* Corresponding author. Correspondence address: Department of Geology, University of Oslo, Blindern, N-0271 Oslo, Norway.
E-mail address: daniel.kohn@geologi.uio.no (D. Koehn).

0191-8141/02/$ - see front matter
PII: S0191-8141(02)00022-6

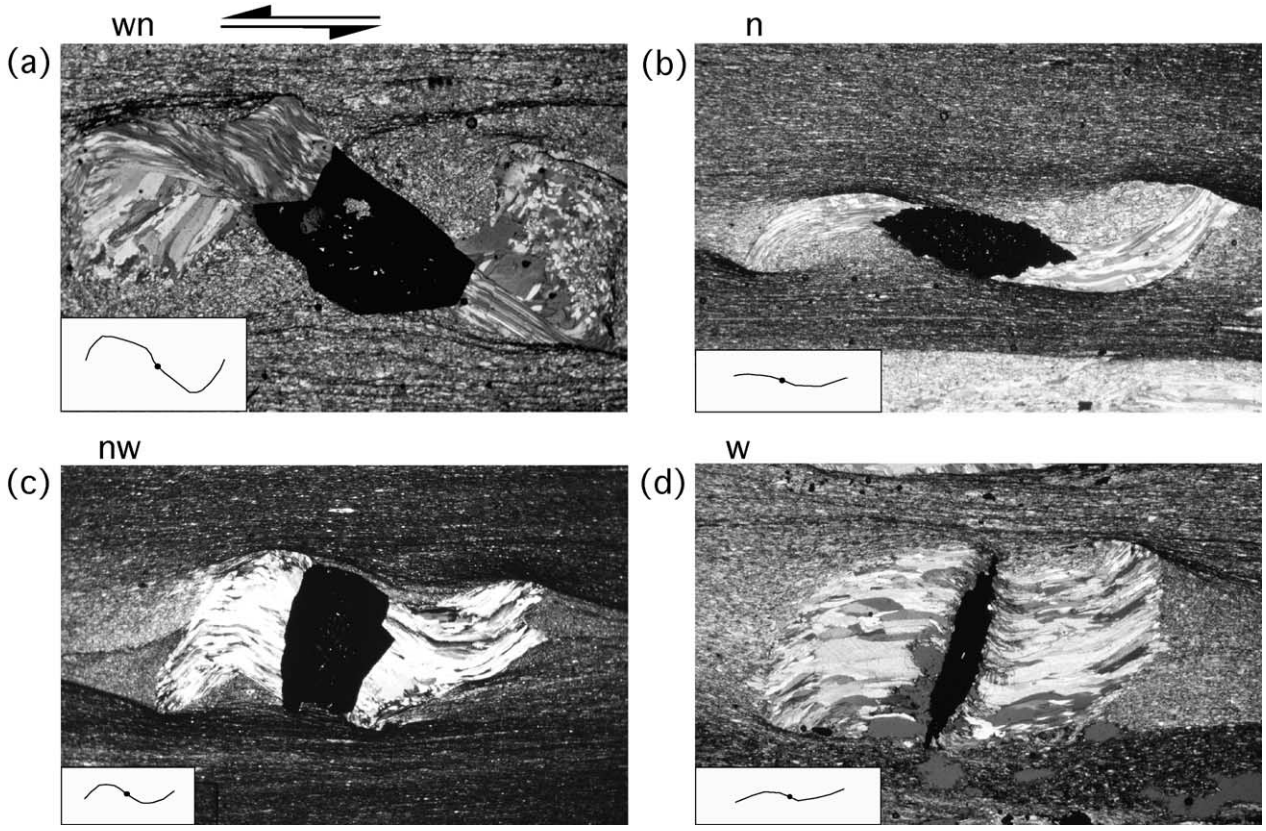

Fig. 1. Micrographs of four strain fringes from the same locality in the northern Pyrenees, Lourdes, France. Shear strain is sinistral. The strain fringes around elongate pyrite crystals show very different final shapes and fibre patterns even though they presumably experienced similar progressive deformation. Object-centre paths are shown in the lower left corner (size 1:3). Width of view is about 8 mm. (a) wn-type fringe, (b) n-type fringe, (c) nw-type fringe, and (d) w-type fringe. See text for explanation.

which includes relative rotation between fringes and core-object (Casey et al., 1983). Observations on natural fringes (Koehn et al., 2001a) and the results of numerical experiments (Koehn et al., 2000, 2001a,b), based on Urai et al. (1991) and Bons (2001) show that displacement-controlled fibres in fringes follow points on the core-object surface. Fibres therefore record relative movement between fringes and core-object and do not necessarily form parallel to extensional ISA. In order to separate translation from rotation components in a two-dimensional analysis Aerden (1996) and Koehn et al. (2000) introduced the concept of *object-centre paths*, which can be determined from natural antitaxial strain fringes. To construct an object-centre path the core-object is moved over a fringe and rotated around its centre in such a way that single points on the surface are always connected to the same displacement-controlled fibres (Koehn et al., 2001b). The trace of the geometric centre of the core-object during this procedure defines the object-centre path (relative translation component) and rotation of the core-object relative to its initial position can be indicated along the path in degrees (relative rotation component). These object-centre paths can be interpreted in terms of strain as well as relative and absolute rotation of fringes and core-object with respect to an external reference frame (Müller et al., 2000; Koehn et al., 2001a) if the assumption is made that incremental opening direction of the fringes is parallel to extensional ISA. However, studies of natural fringes have shown that these structures do not always open parallel to extensional ISA during progressive non-coaxial deformation (Koehn et al., 2001a). Therefore, an investigation of the development of fringe structures as a function of host-rock deformation is essential to determine the reliability of such fibre analyses.

Two numerical studies have been carried out to investigate the development of antitaxial strain fringes during non-coaxial progressive deformation, which include host-rock deformation (Etchecopar and Malavieille, 1987; Kanagawa, 1996). Etchecopar and Malavieille (1987) used a model based on a principle of geometrical best fit between a rigid object and a deformable host-rock. With their method they were able to reconstruct fibre patterns similar to those found in natural examples and they determined finite shear strain and vorticity. Kanagawa (1996) calculated the rotation of fringe structures with respect to an external reference frame during general flow using known equations of rigid body rotation (Jeffery, 1922). He used two models for antitaxial fringe growth where in one he treated fringes and core-object as one rigid object and determined rotation rates from the fringe structure's shape (using a best fit elliptical shape, coupled rotation model) and in the other

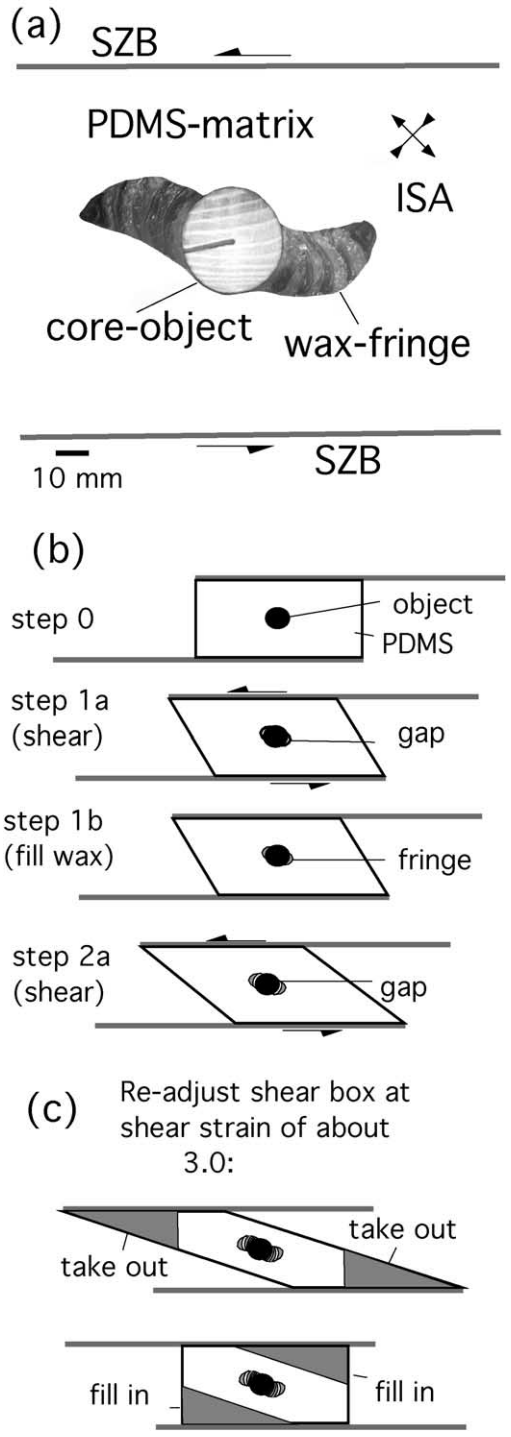

Fig. 2. (a) Photograph of an experimental fringe structure consisting of a wooden core-object and paraffin wax fringes in a simple shear box. Differently coloured slices in the fringes represent different growth events. SZB = shear-zone boundary. ISA = incremental stretching axes. (b) Illustration of the first steps of an experiment. (c) To attain high shear strains the PDMS in the shear box had to be relocated during the experiments. This does not affect the fringe structures.

he decoupled core-object and fringes (decoupled rotation model). He was able to present a fibre curvature analysis that can be used to determine the vorticity of a shear-zone containing strain fringes. However, studies on rigid body rotation of non-interacting objects (e.g. Ghosh and Ramberg, 1976; Jezek et al., 1994; ten Brink and Passchier, 1995; Weijermars, 1997) and of interacting objects (e.g. Ildefonse et al., 1992a,b) have shown that closely spaced rigid objects influence each other's rotation rates. Therefore, the equations of Jeffery (1922) are not necessarily valid for very closely spaced objects, such as a core-object and its two fringes.

In order to test existing models we chose to perform simple analogue experiments as a first attempt to understand the interaction of fringe structure parts and their ductilely deforming matrix. We investigated rotation and translation of fringes with respect to the core-object and rotation of these three rigid bodies with respect to the shear-zone boundary (SZB) in non-coaxial flow to compare the results with previous studies on rigid object rotation. We then calculated incremental rotation and incremental and finite shear strain from object-centre paths determined from the experimental fringes using theoretical methods and compared these values with actual applied rotation and bulk shear strain in the shear box to investigate the reliability of strain fringes for a structural analysis.

2. Experimental procedure

The experiments were performed in a 12-cm-wide simple-shear box where two plexiglas plates acted as SZBs and were displaced parallel to each other (Fig. 2a). The shear-zone had a height of about 5 cm and was about 20 cm long. At the base of the shear-zone we minimized friction by inserting thin pieces of plastic foil. The ends of the shear-zone between the moving plates were restrained by a number of removable small plexiglas plates to prevent outflow of material and other effects of open boundaries (Morgenstern and Tchalenko, 1967; Ramsay and Lisle, 2000). Cylindrical wooden blocks (diameter 2 to 3 cm) of variable shape were used as rigid core-objects and the transparent polymer Polydimethylsiloxane (PDMS) was used to simulate the host-rock. The viscosity of the PDMS used for our studies is 5.0×10^4 Pa s. It has a Newtonian flow behaviour at low differential stress values but strain rate softening takes place at values exceeding about 1000 Pa (Weijermars, 1986). At fast shear-strain rates PDMS behaves elastic. The average shear-strain rate in our experiments was in the order of 0.01 to 0.1 s^{-1}. Therefore, the shear stress was in the order of 500 to 5000 Pa and the material partly behaved non-Newtonian. Close to the rigid wood pieces where the matrix and fringes are pulled away from the core-object PDMS behaved partly elastic.

A wooden core-object was inserted in the middle of the PDMS-matrix. For each fringe growth increment, the matrix

was sheared manually until 2–3-mm-wide gaps formed on the sides of the core-object. The gaps were filled with molten paraffin wax, which was then left to crystallise for a few minutes to become rigid relative to the PDMS-matrix. This procedure was repeated up to 11 times with alternating wax colours (Fig. 2b). The structures were made up of multiple growth events where growth segments were added antitaxially, and therefore mimicked antitaxial strain fringes. In order to achieve high shear-strain, part of the matrix had to be cut out and reassembled periodically (Fig. 2c). Care was taken to ensure that the orientation of core-object and fringes with respect to the edge of the shear-box was not affected by this process. Due to the additional input of wax the shear-zone increases its volume by about 3% during one experiment. In a test-run without rigid objects the internal part of the shear zone showed a slight synthetic rigid body rotation of up to 3° relative to the SZB at a shear strain of five. At the rims of the shear-box PDMS shows localisation of strain so that the internal strain in the shear-box is approximately 10% lower than the externally applied strain.

Object-centre paths of the experimental fringe structures were measured in order to compare the experiments with natural fringes. The paths yield incremental opening directions of fringes with respect to the ISA (ΔOD) and can be used as input to calculate apparent incremental shear strain. These paths can also be used to predict displacement-controlled fibre patterns in the experimental fringes (Fig. 3; Koehn et al., 2001a). However, one has to keep in mind that these patterns are an interpretation, fibres are not directly generated in the experiments. Finally, object-centre paths were used to simulate fibre patterns in the experimental fringes using the program 'Fringe Growth' (Koehn et al., 2000). The numerically created fibre patterns were compared with the natural examples of fringe structures from a shear-zone near Lourdes (France, Fig. 1).

Eleven experiments were performed under simple shear conditions with four different core-objects (Fig. 3). Core-object shapes were circular, square, rectangular and octagonal, the latter two having an aspect ratio of 1.5.

3. Results of the experiments

3.1. Shape of different fringes

In the experiments, different fringe shapes developed under the same external conditions due to different core-object shapes and different orientations of core-objects with respect to the SZB (Fig. 3). The fringe structures in experiments 1 and 2 developed around equidimensional core-objects. In that case, fringe shape is dependent on the number of corners that a core-object has and on the orientation of these with respect to ISA, but shapes of the resulting fringe structures do not differ significantly. However, the initial orientation of the core-object is important if it is elongate. For example core-objects in experiments 4(a,b) have the same final orientation but completely different fringe shapes due to the different initial orientation of their core-objects. Experiment 4(a) produced a fringe structure with a low aspect ratio since fringes initially grew on the long sides of the core-object. In experiment 4(b) fringes started and remained growing on the short sides of the core-object to create a more elongate fringe structure. Since equidimensional objects rotate faster than elongate objects inclined with their long axis at an angle of less than 45° to the shear plane (Ghosh and Ramberg, 1976), the fringes and core-object in experiment 4(a) rotated faster than those of experiment 4(b), which enhanced the difference in final shape of the two fringe structures. In Section 4 we present a classification of fringe shapes related to the initial orientation of elongate core-objects with respect to SZB, based on this study. In some experiments fringes on each side of a core-object have different shape. This is a function of the shape of the initial gap that forms next to the rigid body. The size and width of this gap depends on how fast the PDMS can be detached from the core-object surface, i.e. how much cohesion exists between these two materials.

3.2. Relative rotation between core-object and fringes

We define relative rotation of fringes and core-object as the rotation of the core-object relative to one fringe in accordance to the object-centre path method (Aerden, 1996; Koehn et al., 2001a). In this definition a core-object does not rotate relative to a fringe if the two bodies rotate the same amount relative to ISA even though both rotate around different centres of rotation. Anticlockwise rotation of a core-object relative to a fringe is positive. The experiments show that fringes and core-object can rotate with respect to each other as proposed by Aerden (1996) and Koehn et al. (2000, Fig. 3). However, the values in our experiments are significantly lower than those obtained from natural fringes and most experiments show larger total rotation of fringes than core-objects relative to ISA, which is in disagreement with studies on natural samples (Koehn et al., 2001a). Total relative rotation varied from −30° to 25° for the equidimensional core-objects used in experiments 1 and 2(a,b) with an average total relative rotation of 7°. The relative rotation in experiments 3 and 4 is even less since elongate core-objects tend to interfere more with their fringes so that the average total relative rotation is only −3°. The fringe-structure of experiment 3(b) is an exception: it shows relative rotation of up to −15° even though the core-object is elongate. A possible explanation may be that these fringes grew only on the short sides of the core-object. Therefore, relative rotation of core-object and fringes is not hampered as much as it is in fringe structures where all four sides and two corners of the core-objects interfere with their fringes or where fringes grow only on the long sides of the core-object (experiment 3d).

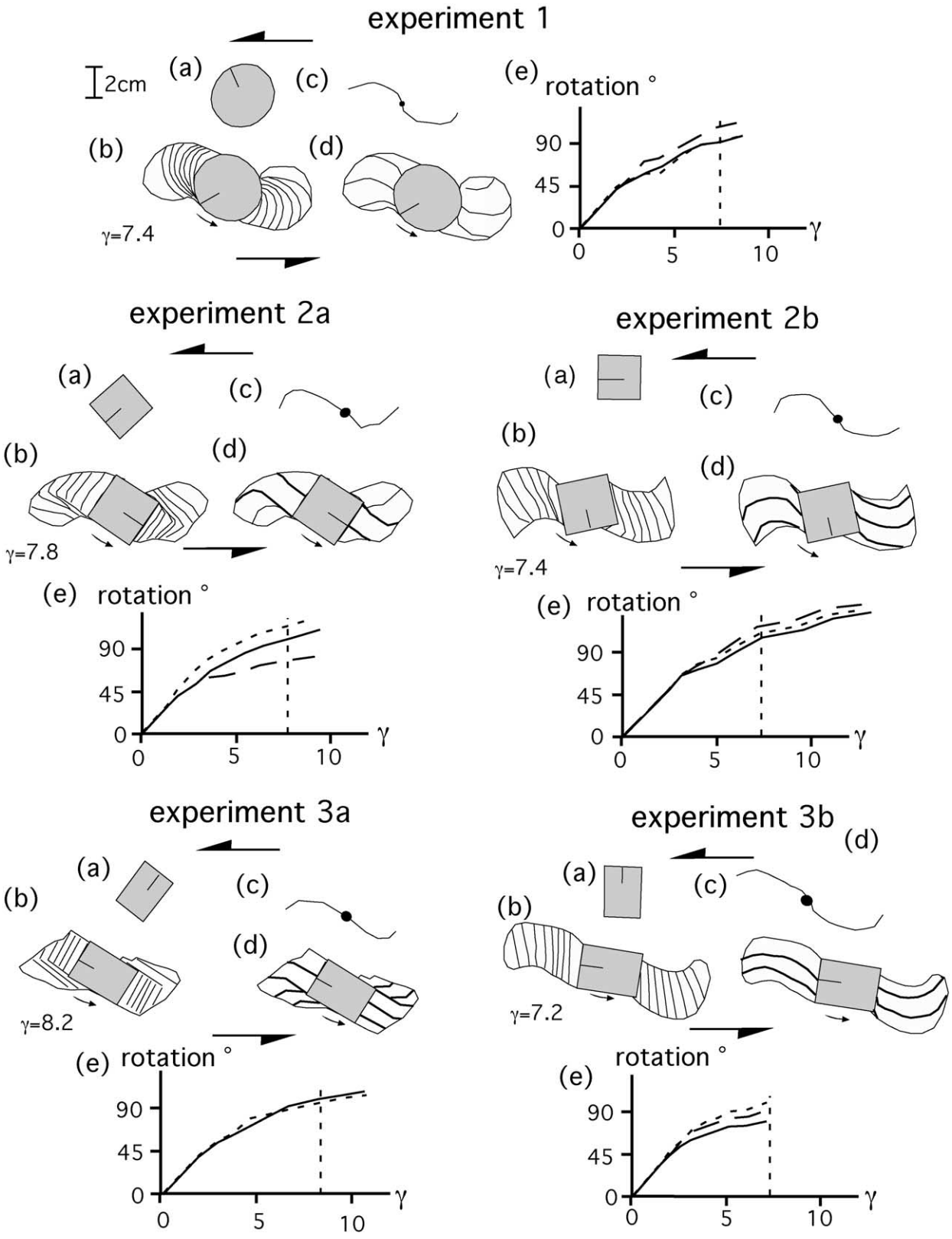

Fig. 3. Results of the experiments. Sinistral shear-zone boundary is horizontal. (a) Initial orientation of the core-object with respect to shear-zone boundary. (b) Fringe structure with lines in fringes indicating different wax-fringe growth events (growth-lines). All fringe structures are shown at about equal shear strain (7.0–8.2). Shear strain (γ) is indicated next to the drawing. (c) Object-centre path determined from (b). (d) Displacement-controlled fibre patterns which would have developed in the fringe structure. (e) Plots of absolute rotation of fringes and core-object with respect to the ISA versus bulk shear strain. Line with short dashes is left fringe, line with long dashes is right fringe, and solid line the core-object. Vertical line indicates stage at which fringe structure is shown in (b) and (d).

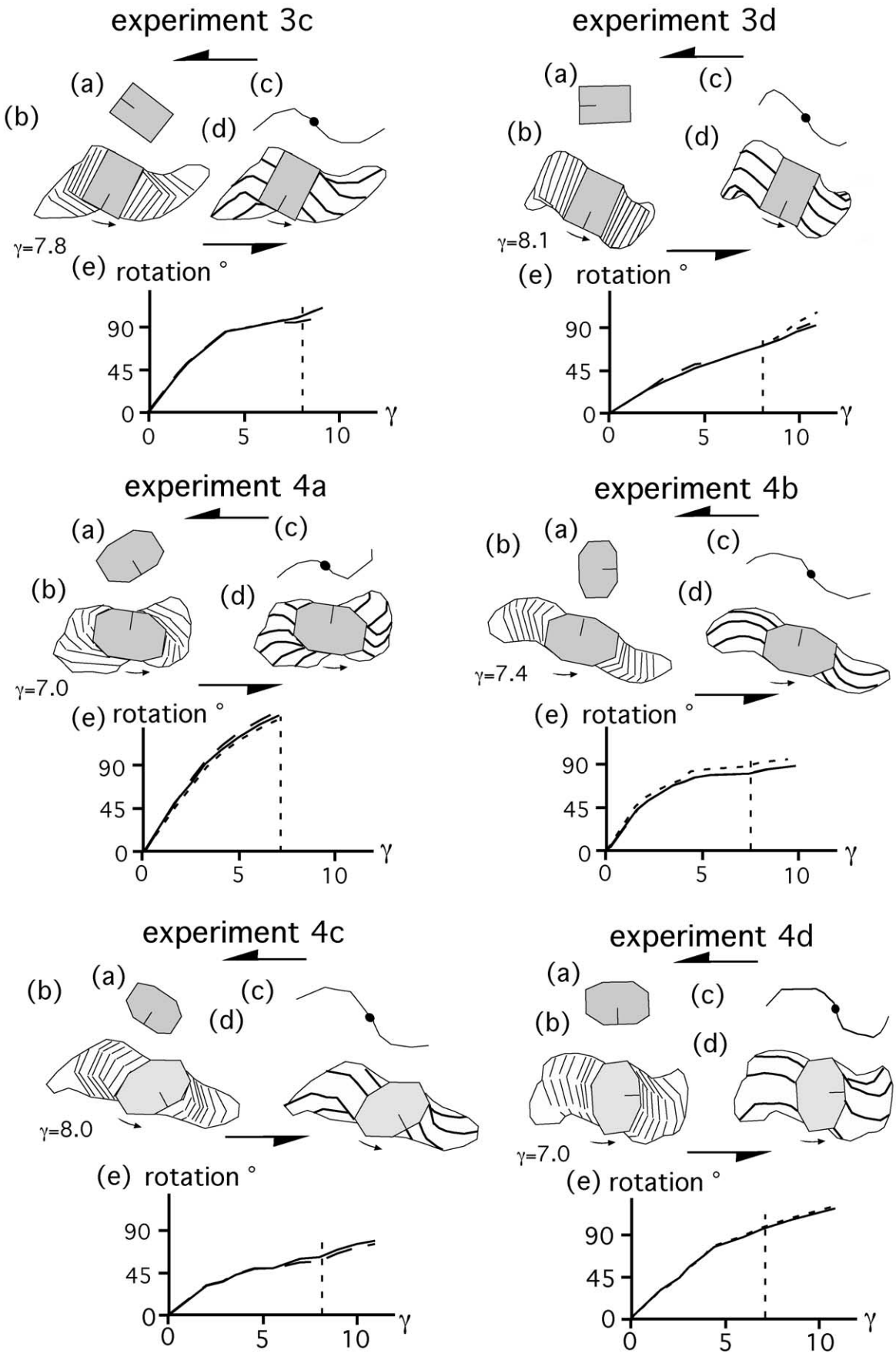

Fig. 3. (*continued*)

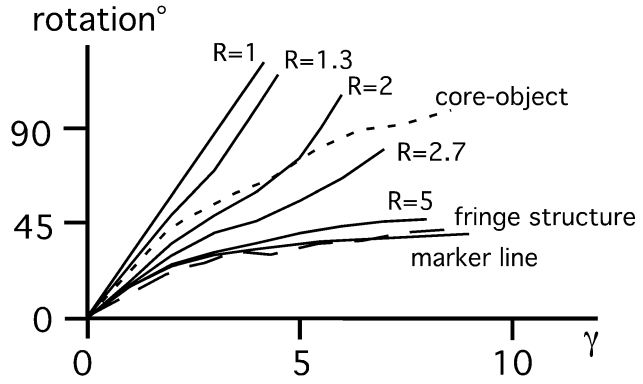

Fig. 4. Plots after Ghosh and Ramberg (1976) for rigid body rotation of objects with different aspect ratios (R) and initial orientation of 45° with respect to the shear plane. The rotation of the round core-object of experiment 1 (Fig. 3) (short dashed line) is similar to the rotation of an object with progressively increasing aspect ratio. The long axis of the fringe structure of experiment 1 (long dashed line) rotates similar to a marker line towards parallelism with the flow plane. Note that the core-object rotates about 2.5 times faster than the long axis of the fringe structure.

3.3. Rotation of core-object and fringes with respect to SZB

Fig. 3e shows plots of fringe and core-object rotation with respect to the SZB versus bulk shear strain. Total shear strain in the experiments varied from 7 to 12 and total rotation from 75° to 140° in the same sense as the sense of shear. All the experiments showed a general decrease in rotation rate of core-objects and fringes relative to the SZB with progressive shear strain. The cause for this is that fringe structures are progressively increasing their axial ratio as they grow during deformation. According to Ghosh and Ramberg (1976), rigid objects with large aspect ratios will rotate with decreasing rates towards the shear plane in simple shear flow. Once an object with an infinitely large aspect ratio is oriented parallel to the shear plane it will stop rotating. None of our experiments showed zero rotation rates but the rotation rates decreased in all experiments as mentioned above. Fig. 4 shows Ghosh and Ramberg's (1976) curves for rigid object rotation in simple shear flow and initial orientation of the long axis of the object at 45° to the shear plane (object parallel to extensional ISA) plotted with curves for the core-object and fringe structure rotation from experiment 1 of this study. We use this initial object orientation, because the orientation of extensional ISA is 45° to the shear plane in our experiments and fringe structures will initially develop an elongate shape in that orientation while they grow. The core-object of experiment 1 behaved like an elongate object of Ghosh and Ramberg (1976) that is progressively increasing its axial ratio (Fig. 4). It is not really clear from our experiments whether the core-object rotation would approach zero or would increase again if experiments were to proceed beyond the end-stage reached, even though some plots show a minor increase in rotation rate (Fig. 3; experiment 3c). The rotation of the long axis of the fringe structure (Fig. 4) with respect to the shear-zone boundary is similar to the rotation of a marker line or an elongate object with an infinitely large aspect ratio, even though the final axial ratio of the fringe structure is only 2.83. The rotation of the fringe structure as a whole seems to influence the rotation rates of core-object and fringes as the latter rotate at approximately 2.5 times the rate of the fringe structure (Fig. 4). This is similar to the 'coupled rotation model' of Kanagawa (1996) that is further discussed in Section 6.

3.4. Fringe opening direction

The incremental opening direction of a fringe is defined as the translation of each fringe relative to the core-object. This translation component is visualised using object-centre paths. Most displacement-controlled fibres in Fig. 3d also show this component, since in our experiments relative rotation of fringes and core-objects is low. Important for structural analysis of strain fringes is the question whether or not fringes open parallel to extensional ISA, so that the youngest object-centre path segments are parallel to this kinematic axis and these paths can be related to an external reference frame (e.g. SZB; Koehn et al., 2001a). In our experiments fringes do not always open parallel to extensional ISA (Fig. 5) due to interference of fringes and core-object, which is illustrated in the following example.

Fig. 5 shows the progressive development of a fringe structure (experiment 3a) and its object-centre path around an elongate core-object. The plot shows the difference between the orientation of the opening direction (ΔOD) of the fringe structure (averaged for both fringes) and the orientation of extensional ISA versus shear strain. Positive values of ΔOD represent anticlockwise orientation with respect to ISA and negative values clockwise orientation. The different stages of fringe growth are marked on the plot. At stage one after a shear strain of 1.8, fringes grew on the long sides of the core-object and ΔOD was 37°. The orientation of the long side of the core-object influenced fringe OD so that OD was almost perpendicular to the surface of the core-object. Because this side rotated towards extensional ISA, OD rotated away from it towards parallelism with the flow plane. The OD became parallel to extensional ISA, once the fringes started growing on the short sides of the core-object in stage 2. The rotation of fringes and core-object around their geometric centres were inhibited from stage 3 on. The movement then partitioned into sliding along the long surface and rotation of the whole fringe structure. Sliding along the long surface of the core-object caused opening perpendicular to the short face, which rotated with the fringe OD away from parallelism with extensional ISA from stages 6 to 9 (Fig. 5). The sudden change in opening direction of fringes between stages 1 and 2 to 4 is indicated by a hook in the object-centre path.

Fig. 6 shows plots of ΔOD versus shear strain for all experiments. One can see that even fringes adjacent to round core-objects do not always open parallel to

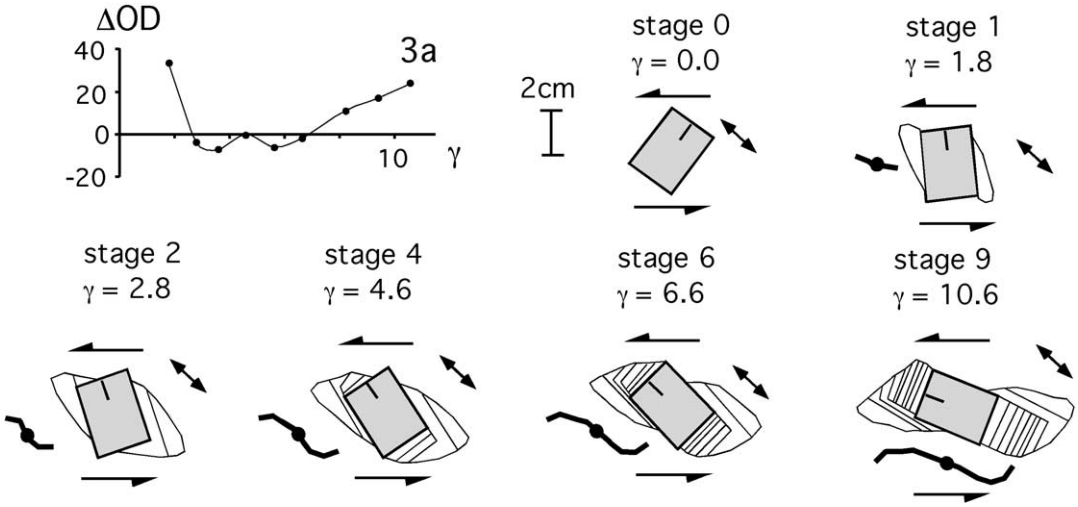

Fig. 5. Plot of the difference between opening direction of fringes of experiment 3(a) and ISA (ΔOD) versus experimental shear strain and development of a wn-type fringe around an elongate core-object in six time-steps. Sinistral shear-zone boundary is horizontal and extensional ISA orientation is indicated by double arrows. The object-centre path represents the fringe-opening direction, which is not always parallel to ISA due to sliding of fringes along the core-object's edge. See detailed explanation in text.

extensional ISA (experiment 1) and develop hooks in object-centre paths. This might be an effect of local strain heterogeneities around the fringe structures, which differ from the average strain field in the shear box and can influence the translation of fringes relative to core-objects. Fringe-opening directions of all the presented experiments vary from 50° to −45° with respect to ISA. Although one can explain non-parallelism of the OD and ISA orientation for an individual experiment (e.g. Fig. 5), there seems to be no systematic relationship between ΔOD and core-object orientation or shape (Fig. 6).

4. Classification of fringes and fibre patterns

4.1. Classification of fringes

Based on our experiments and on comparison with natural fringes, we propose a classification scheme for fringes around elongate core-objects depending on the initial orientation of the core-object's long axis with respect to the shear-zone boundary (Fig. 7). Four main types of geometries can be distinguished indicated by the abbreviations w (wide) and n (narrow) referring to the long and short sides of the core-object, respectively. We did not use l or s as abbreviations because of possible confusion with LS tectonites. (1) *wn-type* fringes (wide–narrow-type, referring to the wide (long) and narrow (short) sides of elongate core-objects; Fig. 3, experiments 3a and 4a) are characterised by early growth of fringes on the long sides of the core-object (initially long sides normal to extensional ISA) and later growth on the short sides; (2) *n-type* fringes (narrow-type) show growth of fringes only on the short sides of the core-object (initially short sides parallel to shear plane; Fig. 3, experiments 3b and 4b); (3) *nw-type* fringes (narrow–wide-

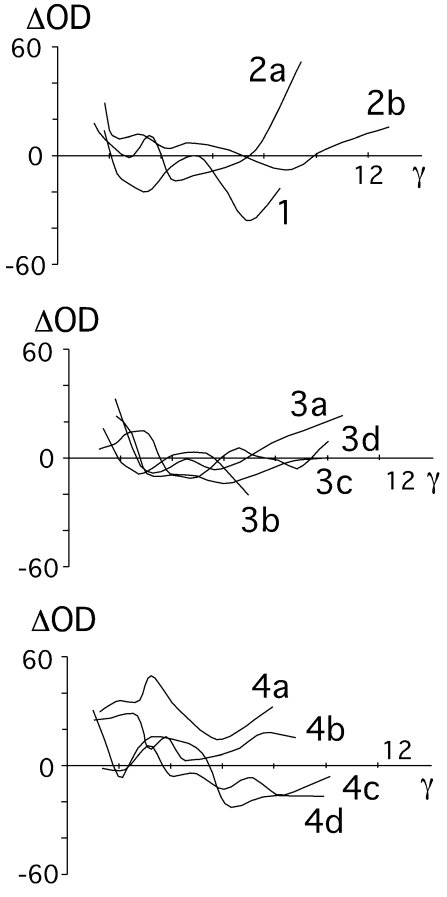

Fig. 6. Plots of the difference in opening direction and ISA orientation (ΔOD) for all experiments versus shear strain. Note that ΔOD varies for all experiments with no consistent relationship to strain, object-shape or object orientation.

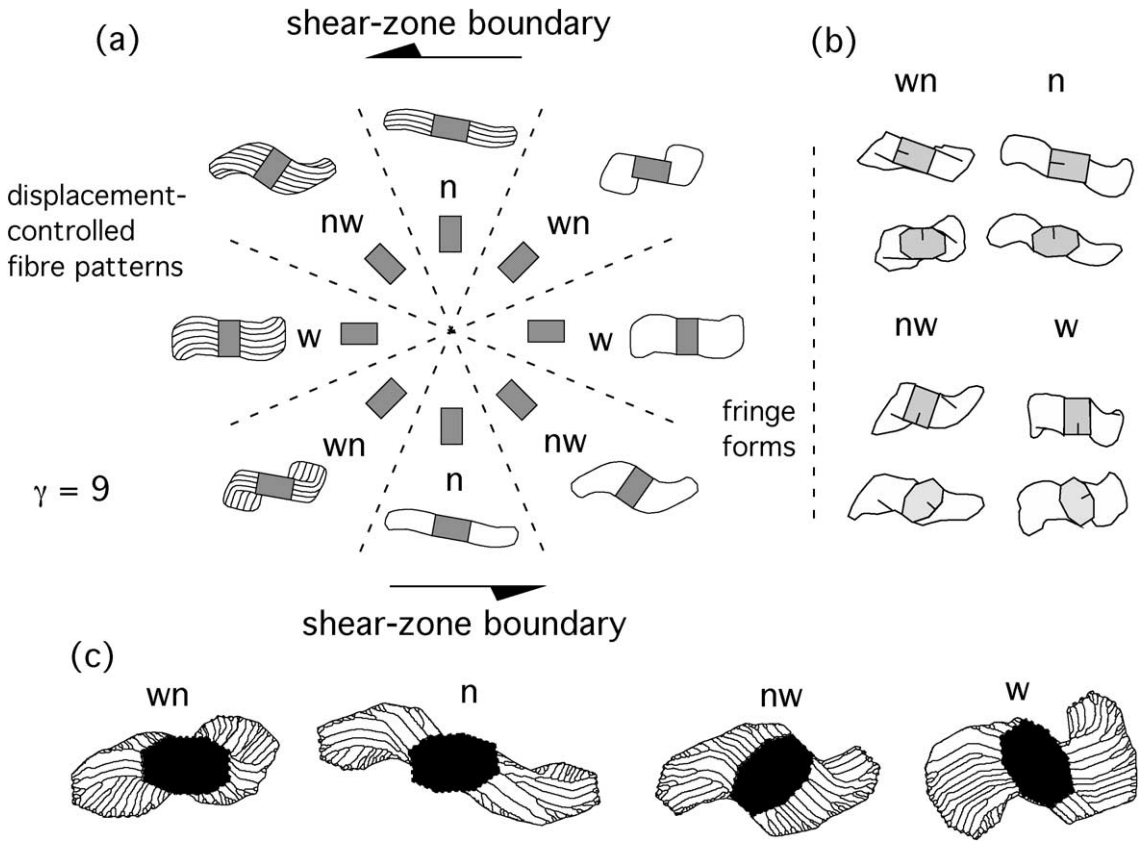

Fig. 7. Proposed classification for fringe structures with elongate core-objects. (a) Schematic drawing of fringe shape and fibre patterns that develop depending on the initial orientation of the core-object's long axis with respect to the shear-zone boundary: n = narrow type, nw = narrow–wide type, w = wide type and wn = wide–narrow type. (b) Fringe structures of experiments 3 and 4 in this classification. (c) Simulation of mainly displacement-controlled fibre patterns in fringes of experiment 4 with the program 'Fringe Growth' of Koehn et al. (2000). Note the similarities with natural examples in Fig. 1.

type) are characterised by an early growth of fringes on the short sides of the core-object (initially short sides normal to extensional ISA) and a later growth on the long sides (Fig. 3, experiments 3c and 4c) and (4) *w-type* fringes (wide-type) show fringe growth mainly on the long sides of the core-object (initially long sides parallel to shear plane; Fig. 3, experiments 3d and 4d).

The classification is based on four end-member geometries, between which intermediate geometries can be expected. With this classification one can deduce the initial orientation of a core-object with respect to ISA from the final fringe shape.

4.2. Simulated fibre patterns

We applied the program 'Fringe Growth' (Koehn et al., 2000) to determine the fibre patterns that would develop in fringes of the shapes that were formed in the experiments. An object-centre path and the shape and orientation of a core-object were used as input. The core-objects were given a rough surface to enforce the development of mainly displacement-controlled fibres. The numerically simulated fibre patterns show a good similarity with natural examples (Fig. 1), and we conclude that our experiments and numerical simulations produced reasonable results and may be good analogues for natural strain fringes such as those found in Lourdes (see also Section 6).

5. Comparison of observed and calculated host-rock deformation

With the experiments presented in this paper we are able to investigate how well strain calculated from fibres in strain fringes compares with the bulk deformation of the matrix material. We use object-centre paths for the interpretations since they can be derived directly from the experiments and can also be calculated from fibres in natural samples. As mentioned earlier displacement-controlled fibres will be equal or similar to object-centre paths in our experiments since relative rotations between core-object and fringes are low. However, the reader has to keep in mind that this method is already an interpretation following the fibre-growth model of Koehn et al. (2000, 2001a,b). We will first use the strain-estimation method of Koehn et al. (2001a) and then discuss alternative methods (Durney and Ramsay, 1973; Ramsay and Huber, 1983; Ellis, 1986).

Koehn et al. (2001a) presented a method to calculate

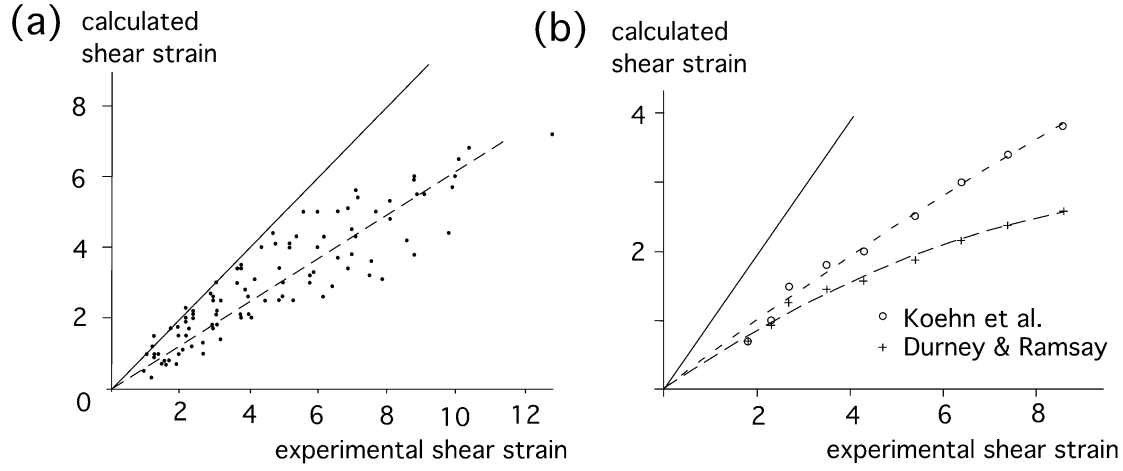

Fig. 8. (a) Plot of experimental shear strain versus estimated shear strain (using the method of Koehn et al., 2001a) for all experiments and different stages of fringe growth. Solid line represents equal experimental and calculated strain. Experimental shear strain is a factor of about 1.7 higher than the calculated one (dashed trend-line). (b) Plot of experimental shear strain of experiment 1 versus estimated shear strain with the method of Koehn et al. (2001a) and Durney and Ramsay (1973).

finite shear strain from object-centre paths using the Mohr circle for infinitesimal plane strain so that

$$\gamma_{\max} = e_1 - e_3 \tag{1}$$

where γ is the shear strain and e_1 and e_3 are the normal strains with

$$e = \frac{\Delta l}{l_0}. \tag{2}$$

If the shear strain is infinitesimally small and the area remains constant, then

$$\mathrm{d}e_3 = -\mathrm{d}e_1 \text{ for } \mathrm{d}\gamma \Rightarrow 0 \tag{3}$$

so that

$$\mathrm{d}\gamma_{\max} = 2\mathrm{d}e_1 \tag{4}$$

(for infinitesimally small strain).

The finite shear strain is obtained from integration along the length of the object-centre path:

$$\mathrm{d}\gamma = 2\mathrm{d}e_1 = \frac{2\mathrm{d}l}{l_0}. \tag{5}$$

where l is the incremental length of the object-centre path and l_0 is the diameter of the core-object. Integration gives:

$$\gamma_{\text{finite}} = 2\int_0^L \frac{\mathrm{d}l}{l_0}. \tag{6}$$

where L is the length along the object-centre path (of the whole fringe structure). For a round object Eq. (6) simplifies to:

$$\gamma_{\text{finite}} = \frac{2}{l_o}L. \tag{7}$$

If the core-object is not round one has to take the sum of infinitesimal small amounts of the object-centre path divided by the length of the core-object parallel to the extensional ISA for that segment according to:

$$\gamma_{\text{finite}} = 2\sum \frac{\Delta l_i}{l_i^0}. \tag{8}$$

Fig. 8a shows the results of the calculated finite shear strain plotted against bulk shear strain in the shear box for all 11 experiments and different progressive fringe growth events. Most points in the plot lie below a reference line for equal experimental and calculated shear strain indicating that the calculated shear strain is generally lower than the bulk shear strain in the shear box.

A linear trend-line for all points running through the origin has a slope of 0.6. To correct the calculated shear strain values these have to be multiplied by a factor k which is equal to one divided by this slope:

$$\gamma = 2k\sum \frac{\Delta l_i}{l_i^0} \tag{9}$$

where $k \approx 1.7$.

Eq. (9) could be used to calculate shear strain from object-centre paths determined from natural fringes but the value of k will have to be determined for natural fringes, e.g. in an area where independent strain markers are available. The value of k may be dependent on how much strain is partitioned in the matrix around the fringe structures (see also Section 6). Note that there is no use to fit a non-linear trendline to the data in Fig. 8a since the deviation of the known data from a linear trend is minor.

Other strain-estimation methods that are commonly used for antitaxial strain fringes are those of Durney and Ramsay (1973) or Ramsay and Huber (1983), and Ellis (1986). The method of Ellis (1986) cannot be used to determine finite strain from the presented experiments since it assumes mechanically passive fibres. This is not the case in our experiments; the wax-fringes are rigid. Fig. 8b shows an

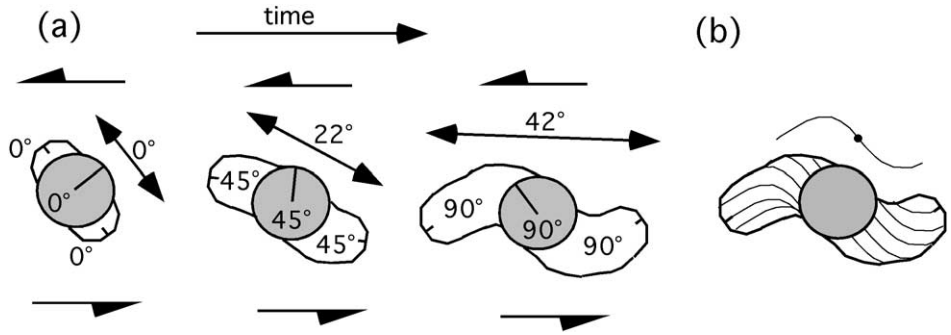

Fig. 9. (a) Progressive rotation of core-object, fringes and the long axis of the fringe structure with respect to ISA representing a 'coupled rotation model'. Fringes and core-object are influenced by the rotation of the fringe structure but rotate faster. Therefore fringes can rotate across the flow plane and more than 90° with respect to ISA even though the long axis of the fringe structure does only rotate up to 45°. Shear sense is sinistral. Large arrow indicates orientation of the long axis of the fringe structure. Rotation angles with respect to initial orientation of fringes, core-object and the long axis of the fringe structure are indicated. (b) Resulting fibre patterns and object-centre path for (a).

application of the method of Durney and Ramsay (1973) and Koehn et al. (2001a) to our experiment 1. The main difference between the two methods lies in the evaluation of l_0 in Eqs. (5)–(9). Koehn et al. (2001a) use the radius or diameter of the core-object in the direction of extensional ISA, whereas Durney and Ramsay (1973) and Ramsay and Huber (1983) use the radius of the core-object plus the length of previously grown fringe-segments in the direction of extensional ISA. Fig. 8b shows that the Durney and Ramsay (1973) method produces values that are deviating from the observed shear-strain values with progressing deformation. Their method gives even lower estimates of finite shear strain than the method of Koehn et al. (2001a). This implies that only the radius or diameter of the core-object should be used as reference length for strain calculations in antitaxial strain fringes.

6. Discussion

Our experiments demonstrate that core-objects and fringes can rotate relative to each other (Aerden, 1996; Koehn et al., 2000). However, the relative rotations determined in our experiments are significantly lower or even of the opposite sense than the ones calculated from natural examples by Koehn et al. (2001a). This is very important for single fibre analysis since the relative rotation of core-object and fringes influences fibre-growth directions. If relative rotation is low this influence can be neglected. Rotation of rigid objects in a matrix will depend strongly on coupling between the bodies and the matrix (cohesion and friction). The differences between our experiments and data from natural fringe-structures suggest that the physical coupling between matrix and bodies is different in both cases suggesting that the experimental relative rotations cannot be extrapolated directly to natural systems. This might have to do with the fact that our experiments are dilatant. If natural fringes are volume-conservative they have more coupling between object and matrix than the ones in our experiments and thus the natural objects might rotate more relative to the SZB.

Our experiments show that complex hook-shaped fibres and object-centre paths as well as several different fringe shapes can develop simultaneously in the same shear-zone in non-coaxial flow and that hook-shaped object-centre paths are not necessarily indicative of polyphase deformation, as suggested by Aerden (1996) and Müller et al. (2000). If the fringe structures from Lourdes shown in Fig. 1 developed during polyphase deformation one would expect that all fringes and fibres show the same characteristic hook, but this is not the case. Therefore we are of the opinion that the fringe structures in Fig. 1 did not grow during polyphase deformation with a sudden (>20°) change of ISA orientation with respect to the fringes as suggested by Aerden (1996) and Müller et al. (2000).

As mentioned in Section 3.3, the rotation of the fringe structure influences rotation rates of fringes and core-objects in a similar way to the 'coupled rotation model' of Kanagawa (1996). The fringes and core-object of a fringe structure rotate at similar decreasing rates with respect to ISA, like elongate objects that increase their axial ratios as mentioned above. The shape of the fringe structure as a whole is therefore more important for the rate of rotation than the shape of the core-object or that of a single fringe. The long axis of a fringe structure changes its orientation with respect to fringes and core-objects progressively since the core-object and each fringe rotate around different centres of rotation. Fringes and core-objects individually rotate more than 45° or even more than 90° with respect to ISA and can thus rotate across the flow plane (Fig. 9) while the fringe-structure as a whole rotates less than 45° during simple shear flow. This can lead to fibres and object-centre paths that are curved more than 90°. In our experiments the fringe structure behaves similar to a boudin train that rotates like a passive marker line towards parallelism with the flow plane. Note that Kanagawa (1996) uses the rotation of the best fit ellipse of the fringe structure for his coupled rotation model, which rotates faster than a markerline.

Our experimental fringes grow slower at the same bulk shear strain than the modelled antitaxial fringes of Kanagawa (1996). An antitaxial fringe-structure of Kanagawa (1996) at a shear strain of 1.8 will have developed at an actual shear strain of 3.14 (using Eq. (7)) and an actual shear strain of 5.34 in our experiments (according to Eq. (9)). As a consequence of this difference, fringe-structure rotation rates in our model (and experiments) are faster than the ones of Kanagawa (1996) and result in different fringe shapes. The reason for this discrepancy lies in the fibre-length calculation of Kanagawa (1996), which follows the Durney and Ramsay (1973) method and thus has a similar effect as the one shown in Fig. 8b. If strain is calculated using this method the difference between bulk strain in our experiments and the calculated values is increasing non-linearly with increasing strain. Calculating the fibre length (Kanagawa, 1996) using the method of Durney and Ramsay (1973) thus results in a non-linear increase in fringe growth with progressive strain. Therefore fringes will grow increasingly faster while the fringe structure increases its axial ratio. This does not happen in our experiments where new fringe segments do not increase their length per strain increment with increasing axial ratio of the fringe structure (for example see Figs. 5 and 8b).

The method of Etchecopar and Malavieille (1987) to model antitaxial strain fringes produces fringes with similar shape and size compared with our experimental fringes. However, fibre patterns in the modelled fringes of Etchecopar and Malavieille (1987) differ from fibre patterns in our model. This has to do with differences in absolute rotation of fringes and core-objects of their method and our experiments. In their method a square core-object has a total rotation of 170° with respect to the SZB at a shear strain of six. The fringes show only a total rotation of 60°. If we compare these values with experiment 2(b) of our study, where the core-object has the same initial orientation with respect to the SZB and the same shape we observe a total rotation of 90° for the core-object at a shear strain of six and a total rotation of the fringes of 100° and 110°. This produces different fibre patterns and can account for the difference between natural examples in Etchecopar and Malavieille (1987) and their simulated fringes (Aerden, 1996). Since our experiments produce results that fit the natural data better than the simulated examples of Etchecopar and Malavieille (1987) we conclude that the fringe rotation in their model is too low. We doubt whether their core-object rotation is more realistic than ours since core-objects of natural fringes seem to show larger total rotation relative to the SZB than their fringes (Koehn et al., 2001a), which is consistent with the model of Etchecopar and Malavieille (1987) but not with our experiments.

An important question is to what extent our experiments can be extrapolated to natural systems. Relative rotation between fringes and core-object seems to be different in nature and our experiments. But the observed fringe forms, object-centre paths and resulting fibre patterns are similar to natural examples. Therefore the experiments should at least give an insight into how natural systems might behave. We certainly need more experiments and computer simulations to successfully test and scale fibre interpretation methods to nature. We then might be able to find the factor k in Eq. (9) to calculate the shear strain of natural fringes (assuming Eq. (9) is correct). In our experiments the factor k depends on tensional strength of the object surface relative to the viscosity of the matrix. For example if the viscosity is low and the matrix sticks to the objects no fringes will develop ($k \rightarrow \infty$). In nature k depends on the viscosity of the matrix, the mobility of the fringe-forming material through the matrix (diffusion limited) or the rate of material growth (rate limited) and the tensional strength of the surface if we believe the surface is a crack. If the viscosity is very high the material will flow around the rigid object and form a delta clast but no fringe. Therefore mobility of the fringe-forming material and viscosity of the matrix must balance to form a fringe. The factor k is unknown for natural fringes at the moment. However, we might be able to find estimates in the future.

7. Conclusions

Experimental two-dimensional modelling of paraffin wax fringes and wooden core-objects in a matrix of PDMS led to the following conclusions:

1. Different fringe shapes can develop in the same shear-zone depending on shape of the core-object and its initial orientation with respect to the ISA.
2. Fringes and core-objects can rotate relative to each other, but show minor relative rotation in our experiments. Fringe structures with elongate core-objects show less relative rotation than those with equidimensional ones.
3. Fringes, core-objects and fringe structures have slower rotation rates with respect to the ISA than single rigid objects with the same aspect ratios.
4. The rotation of the long axis of a fringe structure influences the rotation rate of fringes and core-objects (coupled rotation model).
5. Fringes do not always open parallel to the extensional ISA.
6. Hooks in fibres and object-centre paths do not necessarily represent sudden changes of ISA orientation with respect to fringes, i.e. they do not necessarily represent different phases of deformation.
7. Conventional strain-estimation methods applied to our experiments underestimate bulk shear strain.

Acknowledgements

The authors wish to thank Kyuichi Kanagawa and David Durney for thoughtful reviews. The project was funded by

the DFG Grant Pa 578/3. DK acknowledges additional funding by the European Training Network on dissolution-precipitation processes. We thank Saskia ten Grotenhuis, Sandra Piazolo, Chris Wilson, Klaus Gessner, Domingo Aerden and Chris Hilgers for discussions and suggestions. Anke Wohlers and Ralf Halam are thanked for their help with the experiments.

References

Aerden, D.G.A.M., 1996. The pyrite-type strain fringes from Lourdes (France): indicators of Alpine thrust kinematics in the Pyrenees. Journal of Structural Geology 18, 75–91.

Beutner, E.C., Fischer, D.M., Kirkpatrick, J.L., 1988. Kinematics of deformation at a thrust fault ramp (?) from syntectonic fibers in pressure shadows. In: Mitra, G., Wojtal, S. (Eds.), Geometries and Mechanisms of Thrusting, With Special Reference to the Appalachians. Geological Society of America Special Paper 222, pp. 77–88.

Bons, P.D., 2001. Development of crystal morphology during unitaxial growth in a progressively widening vein: I. The numerical model. Journal of Structural Geology 23, 865–872.

Casey, M., Dietrich, D., Ramsay, J.G., 1983. Methods for determining deformation history for chocolate tablet boudinage with fibrous crystals. Tectonophysics 92, 211–239.

Durney, D.W., Ramsay, J.G., 1973. Incremental strains measured by syntectonic crystal growths. In: deJong, K.A., Scholten, R. (Eds.). Gravity and Tectonics. Wiley, New York, pp. 67–96.

Elliott, D., 1972. Deformation paths in structural geology. Bulletin of the Geological Society of America 83, 2621–2638.

Ellis, M.A., 1986. The determination of progressive deformation histories from antitaxial syntectonic crystal fibres. Journal of Structural Geology 8, 701–709.

Etchecopar, A., Malavieille, J., 1987. Computer models of pressure shadows: a method for strain measurement and shear sense determination. Journal of Structural Geology 9, 667–677.

Fisher, D.M., 1990. Orientation history and rheology in slates, Kodiak and Afognak Islands, Alaska. Journal of Structural Geology 12, 483–498.

Ghosh, S.K., Ramberg, H., 1976. Reorientation of inclusions by combination of pure shear and simple shear. Tectonophysics 34, 1–70.

Ildefonse, B., Launeau, B., Fernandez, A., Bouchez, J.L., 1992a. Effect of mechanical interactions on development of shape preferred orientations: a two-dimensional experimental approach. Journal of Structural Geology 14, 73–83.

Ildefonse, B., Sokoutis, D., Mancktelow, N.S., 1992b. Mechanical interactions between rigid particles in a deforming ductile matrix. Analogue experiments in simple shear flow. Journal of Structural Geology 14, 1253–1266.

Jeffery, G.B., 1922. The motion of ellipsoidal particles immersed in a viscous fluid. Proceedings of the Royal Society of London 102, 161–179.

Jezek, J., Melky, R., Schulmann, K., Venera, Z., 1994. The behaviour of rigid triaxial ellipsoidal particles in viscous flows-modeling of fabric evolution in a multiparticle system. Tectonophysics 229, 165–180.

Kanagawa, K., 1996. Simulated pressure fringes, vorticity, and progressive deformation. In: De Paor, D.G. (Ed.). Structural Geology and Personal Computers. Elsevier Science, Oxford, pp. 259–283.

Koehn, D., Hilgers, C., Bons, P.D., Passchier, C.W., 2000. Numerical simulation of fibre growth in antitaxial strain fringes. Journal of Structural Geology 22, 1311–1324.

Koehn, D., Aerden, D.G.A.M., Bons, P.D., Passchier, C.W., 2001a. Computer experiments to investigate complex fibre patterns in natural antitaxial strain fringes. Journal of Metamorphic Geology 19, 217–231.

Koehn, D., Bons, P.D., Hilgers, C., Passchier, C.W., 2001b. Animations of progressive fibrous vein and fringe formation. Journal of the Virtual Explorer 3, Animations in Geology.

Means, W.D., 1976. Stress and Strain. Springer, Heidelberg.

Means, W.D., 1994. Rotational quantities in homogeneous flow and the development of small-scale structure. Journal of Structural Geology 16, 437–445.

Morgenstern, N.R., Tchalenko, J.S., 1967. Microscopic structures in kaolin subjected to direct shear. Geotechnique 17, 309–328.

Mügge, O., 1928. Ueber die Entstehung faseriger Minerale und ihrer Aggregationsformen. Neues Jahrbuch für Mineralogie, Geologie und Paläontologie 58A, 303–438.

Müller, W., Aerden, D., Halliday, A.N., 2000. Isotopic dating of strain fringe increments: duration and rates of deformation in shear zones. Science 288, 2195–2198.

Pabst, A., 1931. 'Pressure-shadows' and the measurement of the orientation of minerals in rocks. Journal of the Mineralogical Society of America 16, 55–70.

Passchier, C.W., Trouw, R.A.J., 1996. Microtectonics. Springer, Heidelberg.

Ramsay, J.G., Huber, M.I., 1983. The Techniques of Modern Structural Geology, 1: Strain Analysis. Academic Press, London.

Ramsay, J.G., Lisle, R.J., 2000. The Techniques of Modern Structural Geology, Volume 3: Applications of Continuum Mechanics. Academic Press, London.

Spencer, S., 1991. The use of syntectonic fibres to determine strain estimates and deformation paths: an appraisal. Tectonophysics 194, 13–34.

ten Brink, C.E., Passchier, C.W., 1995. Modelling of mantled porphyroclasts using non-Newtonian rock analogue materials. Journal of Structural Geology 17, 131–146.

Urai, J.L., Williams, P.F., Van Roermund, H.L.M., 1991. Kinematics of crystal growth in syntectonic fibrous veins. Journal of Structural Geology 13, 823–836.

Weijermars, R., 1986. Flow behaviour and physical chemistry of bouncing putties and related polymers in view of tectonic laboratory applications. Tectonophysics 124, 325–358.

Weijermars, R., 1997. Pulsating oblate and prolate three-dimensional strains. Computers and Geosciences 29, 17–42.

Wickham, J.S., 1973. An estimate of strain increments in a naturally deformed carbonate rock. American Journal of Science 237, 23–47.

Zwart, H.J., Oele, J.A., 1966. Rotated magnetite crystals from the Rocroi Massif (Ardennes). Geologie en Mijnbouw 45, 70–74.